Published in final edited form as:
J Am Soc Mass Spectrom. 2011 September ; 22(9): 1534–1551. doi:10.1007/s13361-011-0185-x.

Gas-Phase Fragmentation Analysis of Nitro-Fatty Acids

Gustavo Bonacci[1], **Eliana K. Asciutto**[2], **Steven R. Woodcock**[1], **Sonia R. Salvatore**[1], **Bruce A. Freeman**[1], and **Francisco J. Schopfer**[1]

[1]Department of Pharmacology and Chemical Biology, University of Pittsburgh, E1340 BST, 200 Lothrop St., Pittsburgh, PA, 15261, USA

[2]Department of Chemistry and Biochemistry, Center for Computational Sciences, Duquesne University, Pittsburgh, PA, USA

Abstract

Nitro-fatty acids are electrophilic signaling mediators formed in increased amounts during inflammation by nitric oxide and nitrite-dependent redox reactions. A more rigorous characterization of endogenously-generated species requires additional understanding of their gas-phase induced fragmentation. Thus, collision induced dissociation (CID) of nitroalkane and nitroalkene groups in fatty acids were studied in the negative ion mode to provide mass spectrometric tools for their structural characterization. Fragmentation of nitroalkanes occurred mainly through loss of the NO_2^- anion or neutral loss of HNO_2. The CID of nitroalkenes proceeds via a more complex cyclization, followed by fragmentation to nitrile and aldehyde products. Gas-phase fragmentation of nitroalkene functional groups with additional γ or δ unsaturation occurred through a multiple step cyclization reaction process, leading to 5 and 6 member ring heterocyclic products and carbon chain fragmentation. Cyclization products were not obtained during nitroalkane fragmentation, highlighting the role of double bond π electrons during NO_2^- rearrangements, stabilization and heterocycle formation. The proposed structures, mechanisms and products of fragmentation are supported by analysis of ^{13}C and ^{15}N labeled parent molecules, 6 different nitroalkene positional isomers, 6 nitroalkane positional isomers, accurate mass determinations at high resolution and quantum mechanics calculations. Multiple key diagnostic ion fragments were obtained through this analysis, allowing for the precise placement of double bonds and sites of fatty acid nitration, thus supporting an ability to predict nitro positions in biological samples.

Keywords

Nitrated fatty acid; LNO_2; OA-NO_2; Nitroalkene; Nitroalkane; Nitro-oleic acid; Nitrolinoleic acid; NO_2-FA

Introduction

Nitro-fatty acids (NO_2-FA) are ubiquitous molecules formed upon the nitration of unsaturated fatty acids by nitric oxide and nitrite-derived species, predominantly nitrogen dioxide [1, 2]. Following initial reports of *in vitro* formation, NO_2-FA were found to occur

Correspondence to: Bruce J. Freeman; freerad@pitt.edu, Francisco J. Schopfer; fjs2@pitt.edu.

Electronic supplementary material The online version of this article (doi:10.1007/s13361-011-0185-x) contains supplementary material, which is available to authorized users.

under physiological conditions in animal and human blood, urine and tissues [3-8] and to mediate a variety of signaling mechanisms [9-11].

The detection of biologically-active fatty acid metabolites was initially performed by GC-MS, which added lengthy sample derivatization steps to protect labile groups and make fatty acid derivatives more volatile. Although some biologically active lipid-derived species are still being measured by GC-MS (i.e. isoprostanes [12]), most of the protocols migrated to LC-ESI-MS methods because of shorter sample work-up times and increased preservation of unstable and reactive products. In particular, electrophilic NO_2-FA decay at accelerated rates under the basic conditions of some derivatization reactions, while acid-catalyzed nitration of native fatty acid occurs at low pH in the presence of nitrite, generating artifactual nitrated fatty acids. These issues significantly complicate the value of GC-MS-based sample analyses. The “soft” ionization of ESI-based procedures provides a more precise and sensitive approach for analyzing samples using triple quadrupole and linear ion trap mass spectrometers. Because of its versatility, LC-ESI-MS has been the preferred method for the detection, analysis and quantification of NO_2-FA. In this regard, NO_2-FA analysis has been performed in negative ion mode using tandem mass spectrometry, with collision induced dissociation (CID) energies that maximize the charged and neutral losses of NO_2^- and HNO_2 (35eV). This approach does not provide data about regioisomer composition or distribution [3, 4, 13, 14]. Although this technique is of value for quantification, additional structural information about specific regioisomer distribution is lost. Thus, structural confirmation of biological samples has relied on the synthesis and comparison to ^{13}C or ^{15}N labeled internal standards [4, 15-17], resulting in a number of limitations. First, no structural differences are observed upon fragmenting nitroalkenes versus nitroalkanes, since both yields the same 46 Da product ion. This is of relevance, since in rodents and humans, nitroalkanes are a metabolite of nitroalkenes [14] and the signaling actions of nitroalkenes differ widely from nitroalkanes [9, 15, 18, 19]. In this vein, different nitroalkene regioisomers have specific peroxisome-proliferator activated receptor γ (PPARγ)-mediated signaling actions, highlighting the need for mass spectrometric methods that aid in their elucidation [20, 21].

Nitro-fatty acids are ideal candidates for LC-ESI-MS characterization and quantification because of the ease of ionization of the carboxylic acid and facile loss of characteristic NO_2 group. Characterization of vicinal nitro-hydroxy fatty acids, a product of nitroalkene hydration, has been simplified by the electron withdrawing properties of hydroxyl (OH) groups, allowing for precise prediction of fragmentation products [3, 22]. The structural characterization and fragmentation analysis of nitroalkenes was attempted using collision induced fragmentation without conclusive results [23]. So far, the strongest mass spectrometric structural analysis of NO_2-FA is based on Li^+ adduction, that helps direct fragmentation and analysis of products in the positive ion mode [24]. Although this can provide revealing structural information, poor sensitivity induces limitations in biological sample analysis.

CID is a fragmentation technique based on energizing an ion by collision with a neutral gas (helium for ion trap and nitrogen for triple quadrupole spectrometers). Upon gas collisions with the ions of interest, translational energy is transferred as vibrational and rotational energy into the ion, which induces bond dissociation. This fragmentation is generally heterolytic and predominantly generates even-electron ion pairs, although radical ions are formed under some circumstances [25]. While rules to explain and predict fragmentation patterns have been established, they are not consistently reliable for unambiguous identification of unknown compounds [26]. This motivated better understanding of the fragmentation of nitroalkenes to provide the structural insight needed for biological sample analysis. Herein we characterize the fragmentation pathways of NO_2-FA containing the

following groups: nitroalkanes, nitroalkane-alkenes, nitroalkenes and bis-allylic nitroalkenes. This study defines an unprecedented gas-phase fragmentation pathway for nitroalkenes involving remote oxygen transfer, supported by the use of ^{13}C labeled standards and ^{15}N nitroalkenes. Fragmentation ions were characterized in the negative ion mode using two mass spectrometers (triple quadrupole and linear ion trap) and the proposed fragmentation pathways were analyzed by semiempirical and quantum mechanics calculations. These findings thus permit more precise prediction of fragment ions following MS/MS of unknown NO_2-FA and their metabolites.

Materials and Methods

Solvents were obtained from Burdick and Jackson. All other materials and reagents were obtained from Sigma-Aldrich (St. Louis, MO, USA). All NO_2-FA were synthesized as previously [4, 27]. Nitroalkanes were obtained by selectively reducing nitroalkenes to the corresponding nitroalkane using $NaBH_4$.

Chromatography

Isomers were separated previous to mass spectrometry analysis using a C18 reverse phase column (2×150 mm, 3 μm particle; Phenomenex) at a 250 μL/min flow rate. Nitrated fatty acids were injected at 65% A (H_2O+0.1% acetic acid), the gradient was held for 3 min, and then the gradient was ramped to 20% A in 45 min. The column was washed at 100% B (acetonitrile+0.1% acetic acid), held for 4 min, and switched back to initial conditions for reequilibration for 5 min.

Mass Spectrometry

The CID spectra were recorded using a LTQ Velos Orbitrap equipped with a HESI II electrospray source. The following parameters were used: source temperature 400 °C, capillary temperature 360°C, sheath gas flow 30, auxiliary gas flow 15, sweep gas flow 2, source voltage −3.3 kV, S-lens RF level 44 (%). The instrument FT-mode was calibrated using the manufacturers recommended calibration solution with the addition of malic acid as a low *m/z* calibration point in the negative ion mode.

Fragmentation Yield Calculation

Areas under the curve for all the reported specific MRM transitions were calculated at different concentrations in the presence of internal standard. A standard curve for each NO_2-OA and NO_2-LA isomer was created for each specific transition by plotting area ratios (analyte specific MRM peak area/internal standard peak area) against concentration ratio (analyte concentration/internal standard concentration) and slopes were calculated. Slopes were used as an index of detection efficiency for each particular product ion.

Computational Approaches

To test structural candidate fragments, the structures were built using the MOE program [28]. Energies of all candidate molecules were calculated using the semiempirical PM3 method [29]. Selected candidates were fully investigated using ab initio calculations. The structure of each fragment was optimized using Gaussian 09 [30] at the B3LYP level of theory, with the triple split valence 6-311G basis set. Zero point vibrational energies (ZPE) corrections were also calculated at the same level of theory.

Results and Discussion

The first approach to structural elucidation by mass spectrometry was to study the CID-induced fragmentation spectra of the nitro-oleic acid (NO_2-OA) regioisomers 9-nitro-octadeca-9-enoic acid (9-NO_2-OA) and 10-nitro-octadeca-9-enoic acid (10-NO_2-OA).

Negative Ion Mode CID-MS/MS of 9-NO_2-OA, and 10-NO_2-OA

The ESI-MS-MS mass spectrum of the 9-NO_2-OA $[M - H]^-$ in negative ion mode and at collision energies of −35 eV (using a 4000 Qtrap tandem mass spectrometer, Applied Biosystems) showed the formation of the following ions at *m/z* 308.2 $[M - H_2O]^-$, 290.2 $[M - 2H_2O]^-$, 279.2 $[M - HNO_2]^-$, 246.2 $[M - 2H_2O - CO_2]^-$ (Figure 1), as previously [3]. Similar high collision energies have been previously used in tandem mass spectrometers for the quantification of nitro-fatty acids [3, 6, 13, 14, 31], for sensitivity optimization of MRM transitions 324.2/46, and 324.2/279.2. The MS^3 analysis of the aforementioned product ions was similar for the 9-NO_2-OA and the 10-NO_2-OA isomers and was used to evaluate the charge site and charge mobility during the fragmentation process. The MS^3 fragmentation of 326.3 *m/z*→308.2 *m/z* resulted in loss of H_2O (*m/z* 290.2), CO_2 (*m/z* 264.2) and CO_2+H_2O (*m/z* 246.2). MS^3 fragmentation of 326.3 *m/z*→279.2 *m/z* resulted in loss of H_2O (*m/z* 261.2) and loss of CO_2 (*m/z* 235.1); MS^3 fragmentation of NO_2-[$^{13}C_{18}$]OA for the following product ions: 344.3 *m/z*→326.2 *m/z* resulted in loss of H_2O (*m/z* 308.2), HNO_2 (*m/z* 279.2) and HNO_2+H_2O (*m/z* 261.2), and 344.3 *m/z*→308.2 *m/z* for loss of $^{13}CO_2$ (*m/z* 263.2). Despite a high sensitivity, no specific structural information can be extracted from these product ions. Lowering the collision energy in the triple quadrupole MS to the 15–20 eV range results in the appearance of additional ions that are not apparent at higher collision energies. This motivated characterization of these ions using a high resolution ion trap mass spectrometer in order to gain structural information and to obtain MS^3 fragmentation spectra. Unlike triple quadrupole-MS at low collision energies (17 eV), ion traps favor non-chain-breaking products ions (HNO_2, H_2O, and CO_2 losses) over chainbreaking fragmentations resulting in a lower yield of overall product ions containing structural information.

9-NO_2-OA

Fragmentation of 9-NO_2-OA results in formation of an ion at *m/z* 168.1 fragment (Figure 1A and Scheme 1A). Its structure was confirmed by accurate mass measurement, showing a mass of 168.1026 that corresponds to an elemental composition of $[C_9H_{14}O_2N]^-$. This was further confirmed by the fragmentation of 9-NO_2-[$^{13}C_{18}$]OA, which gave an ion with a mass of 177.1326, corresponding to $[^{13}C_9H_{14}O_2N]^-$ (Figure 1B). MS^3 fragmentation of the 326.2 *m/z*→168.1 *m/z* ion resulted in the loss of CO_2 (*m/z* 124.1132), confirming that the 168.1 fragment consisted of nine carbons including the carboxylate end of the molecule and no oxygen atoms being lost from the carboxylic acid during the initial chain fragmentation, while both oxygen atoms from the nitro group were transferred to neutral products ions.

10-NO_2-OA

The MS^2 analysis of 10-NO_2-OA shows the formation of a specific ion at *m/z* 169.0864, with a calculated atomic composition of $[C_9H_{13}O_3]^-$ (Figure 1C, Scheme 1B). Further MS^3 analysis of this fragment shows a loss of CO_2 (*m/z* 125.0977, corresponding to a molecular composition of $[C_8H_{13}O]^-$ with *m/z* 125.0961), confirming that this product ion contains the carboxylic acid end. Fragmentation of 10-NO_2-[$^{13}C_{18}$]OA, resulted in the formation of the expected 178.1167 fragment corresponding to $[^{13}C_9H_{13}O_3]^-$ (Figure 1D).

NO_2-OA Fragmentation Mechanism

The proposed mechanism for the carbon chain fragmentation directed by the nitroalkene in the absence of neighboring double bonds is shown for 9-NO_2-OA (Scheme 2). The steps proposed begin with initial rearrangement of the nitro group (see Scheme 2 sidebar), possibly via an unstable three-member dioxaziridine ring, to form a peroxynitroso species, followed by a 1,3-cycloaddition of this moiety with the carbon–carbon double bond to form a 1,2,3-dioxazole intermediate. This pentacycle is labile to intramolecular retro-1,3-cycloaddition Criegee-like fragmentation reaction to form a nitrile group (C≡N) and an unstable carbonyl peroxide zwitterion (C=O–O^-) that rapidly loses water through proton transfer to form the corresponding α-, β-unsaturated nonyl aldehyde (C=O). The same mechanism operating symmetrically describes the 10-NO_2-OA fragmentation pathway (Scheme 1B). The nitroalkene is sufficiently equidistant from both the methyl and carboxylate termini, thus it is assumed that there are no significant directing effects or interactions.

Negative Ion Mode CID-MS/MS of NO_2-LA

Similar to NO_2-OA, the MS^2 spectra of NO_2-LA (*m/z* 324.2) at high collision energies (−35 eV) showed the main neutral losses of H_2O, 2 H_2O, HNO_2, and minor losses of 3 H_2O, H_2O +CO_2 and 2 H_2O+CO_2 resulting in the following product ions at *m/z* 306.2, 288.2, 277.2, 270.2, 262.2, 244.2 respectively (Figure 2A, C, and Figure 3A, C). The main losses of H_2O derive, as for NO_2-OA, from condensation reactions involving the oxygen atoms present in the NO_2 group. This is further confirmed by the MS^3 analysis of 324.2 *m/z*→306.2 *m/z* and→288.2 *m/z* that result in the main loss of CO_2, indicating an intact carboxylate group after the initial two consecutive water losses, thus representing a non-chain-breaking fragmentation pathway similar to NO_2-OA. Fragmentation of NO_2-[$^{13}C_{18}$]LA displayed same neutral losses observed for NO_2-LA as follows: 324.3 *m/z* [M – H_2O]$^-$, 306.2 *m/z* [M – 2H_2O]$^-$, 288.2 *m/z* [M-3H_2O]$^-$, 295.2 *m/z* [M – HNO_2]$^-$, 279.2 *m/z* [M – H_2O-$^{13}CO_2$]$^-$, 261.2 *m/z* [M – 2H_2O-$^{13}CO_2$]$^-$ (Figure 2B, D, and Figure 3B, D). Again, the MS^3 spectra of the 306.3 and 288.2 ions confirmed the preferential condensation reaction involving the oxygen atoms of the NO_2 group since the main MS^3 fragment showed loss of $^{13}CO_2$ group.

Fragment Characterization of NO_2-LA

9-NO_2-LA—Using an online HPLC, the mixture of 4 NO_2-LA positional regioisomers (9-NO_2-LA, 10-NO_2-LA, 12-NO_2-LA, and 13-NO_2-LA) was chromatographically resolved. NO_2-LA positional isomers have been previously described and confirmed by NMR [4, 32]. The CID fragmentation of 9-NO_2-LA resulted in the formation of three main product ions containing structural information with *m/z* values of 168.1, 210.1, and 224.1 (Figure 2A). Thus, the presence of a *bis*-allylic interrupted diene favored additional fragmentation pathways (formation of 210.1 and 224.1 *m/z* product ions), not observed for 9-NO_2-OA. The proximity of an electron-rich π bond to the highly electron withdrawing nitroalkene and the nitro group itself make possible a rich array of productive mechanisms. The mechanistic pathway leading to the formation of an ion with *m/z* 168.1 is common between 9-NO_2-OA and 9-NO_2-LA and corresponds to a cleavage of the C9–C10 double bond, with a net transfer of one or both oxygens from the NO_2 group to its β carbon (C10) (Schemes 1, 2, and 3A).

As a first approach to understanding the fragmentation mechanism, we investigated structural candidates for the ion *m/z* 168.1 (168.1026, molecular composition [$C_9H_{14}O_2N$]$^-$). The candidate products, displayed in Supplementary Scheme 1, were proposed based on the molecular composition and structure of 9-NO_2-LA. Relative energies of predicted fragments were calculated using the PM3 semiempirical approach [29]. From this preliminary energetic analysis, we discarded the structures having the greatest energies

and performed high accuracy energy calculations using Gaussian 09 [30] on the two lowest energy structures (Scheme 4, ions 2 and 3, Table 1). We found that unsaturated imine 2 has a total energy 14.1 kcal/mol higher than nitrile 3. The product ion with lowest energy (3) was used as the endpoint product ion to define the fragmentation mechanism. Based on the initial structure, product ions, energetic analysis and fragmentation mechanisms, we propose for 3 a fragmentation pathway similar to an ozonolysis mechanism (Scheme 5). This is initiated by a nitro-peroxynitroso rearrangement of the oxygen atoms on the nitro group to form the charged peroxynitroso species shown (again possibly via dioxaziridine rearrangement), followed by an intramolecular 1,3-cycloaddition on the neighboring carbon–carbon double bond to form the intermediate five-member ring 1,2,3-dioxazole (analogous to the well-known molozonide). This is followed by a posterior fragmentation by retro-1,3-cycloaddition of the 5 member ring (by analogy to the oxidative cleavage Criegee intermediate) to an aldehyde and a nitrile *N*-oxide. Upon relative rotation of the aldehyde and nitrile oxide to a preferable conformation, a second 1,3-cycloaddition generates a new five-member ring 1,4,2-dioxazole. Finally, a 1,2-hydride shift concomitant with a last retro-1,3-cycloaddition forms a β-, γ-unsaturated nonenoic acid and a charged nitrile nonanoate (3), which is detected with a mass of *m/z* 168.1.

The ion at *m/z* 210.1 (210.1132, molecular composition $C_{11}H_{16}O_3N$) corresponds to a chain breakdown at the C11–C12 bond with the generation of a five-member ring (isoxazole) product, while the product ion at 224.1 *m/z* (224.1289, molecular composition $C_{12}H_{18}O_3N$) represents a chain fragmentation at the C12–C13 bond along with the formation of a six-member heterocycle (4H-1,2-oxazine) (Schemes 3A, 6).

The fragmentation of the 9-NO_2-[$^{13}C_{18}$]LA confirmed a product ion containing 9, 11, and 12 carbons corresponding to ions at *m/z* 177.1 (177.1326, molecular composition $[^{13}C_9H_{14}O_2N]^-$), 221.1 (221.1505, molecular composition $[^{13}C_{11}H_{16}O_3N]^-$), and 236.1 (236.1688, molecular composition $[^{13}C_{12}H_{18}O_3N]^-$), respectively (Figure 2B). For structural elucidation, a similar approach as for the 168.1 *m/z* was used. Using the PM3 semiempirical method, energy values were calculated for several possible product structures associated with the *m/z* 210.1 ion (Supplementary Schemes 1 and 2). Fragments having lowest energies among each group were considered further. The ion product 7 shows the lowest energy (12.3 kcal/mol lower than 6, Table 1). With regard to the non-charged product ions, density functional calculations reveal that Structure 8 (Scheme 6, Table 1) has the lowest energy, 9.3 kcal/mol and 11.9 kcal/mol lower than the other non-charged fragments tested (9 and 10, respectively). For this reason, we selected Structures 7 and 8 as the candidate product ions for which the fragmentation pathway is going to be elucidated. The proposed mechanism of fragmentation to form 7 and 8 is shown in Scheme 7. This involves an initial proton abstraction or transfer from the labile *bis*-allylic methylene unit to the oxygens of the nitro, then a subsequent molecular internal rotation to realign the nitro group for an intramolecular 1,3-cycloaddition of the nitronate species onto the proximal carbon–carbon double bond (β, γ to the nitro) at the γ position, generating the five-member ring isoxalole-2-ol. A posterior retro Diels-Alder addition reaction (Scheme 7 sidebar) cleaves the final isoxazole (*m/z* 210.1), while simultaneously forming the new σ bond between the proximal alcohol and vinyl groups. This enol spontaneously generates an aldehyde after rapid keto-enol tautomerization to the thermodynamically-preferred isomer.

For the product ion *m/z* 224.1, initial calculations (Supplementary Scheme 1) indicated that the structures with lower energies corresponded to 11 and 12 (Scheme 8). Accurate energy calculations confirmed semiempirical data showing that Structure 11 had the lowest energy, followed by Structure 12, 9.6 kcal/mol greater. A fragmentation mechanism for product ion 224.1 *m/z* is presented in Scheme 9. The initial intramolecular 1,3-cycloaddition is followed by a retro 1,3-cycloaddition, which forms an aldehyde and a hexacyclic ylide (*m/z* 224.1)

that is further stabilized by a proton transfer and tautomerization to a more stable 4H-1,2-oxazine. Evidently, the relative placement of the nitro group and alkene are sufficiently distant, and the carbon chain sufficiently flexible, for these intramolecular additions to proceed. Note also the low energy differences calculated between the oxazine isomers. A summary of the structures of the product ions for 9-NO_2-LA is shown in Scheme 3A.

10-NO_2-LA—The CID fragmentation of 10-NO_2-LA gave three characteristic ions with *m/z* values of 182.1, 224.1, and 238.1 (Figure 2C, Scheme 3B), thus showing an overall average shift of 14.0154 with respect to the 9-NO_2-LA that corresponds to a methylene group (14.01510). These three ions contain relevant structural information and their molecular composition is consistent with 10, 12, and 13 carbon, respectively, as confirmed by accurate mass determination. Analysis of 10-NO_2-[$^{13}C_{18}$]LA showed the expected fragments corresponding to ions with masses 192.1, 236.1, and 251.1 (Figure 2D), further confirming the molecular compositions. Moreover, this indicates that the fragmentation pathways occur analogously in the 1,4-skipped diene whether the nitro group is located at α-, β-; δ-, ε-(exterior, e.g., 9-NO_2-LA) as well as at α-, β-; γ-, δ-(interior, e.g., 10- NO_2-LA) relative positions in the 1,4-skipped diene motif with respect to the NO_2 group, resulting in products with an additional methylene group. No space charge constraints affecting the proposed fragmentation mechanism were observed when 9-NO_2- and 10-NO_2-LA regioisomers were compared.

12-NO_2-LA—It was hypothesized that both 12- and 13-NO_2-LA would fragment following the same mechanisms described for the 9-NO_2- and 10-NO_2-LA regioisomers. Thus, analysis of product ions would aid in the structural characterization of the neutral fragments arising from the fragmentation of 9-NO_2- and 10-NO_2-LA, based on the fact that in all cases, the charge remains locked at the carboxylate anion terminus and that these molecules have interior relative symmetric structures with regard to nitro and alkene locations. Energy calculations for the neutral fragmentation products were already performed for 9-NO_2-LA (Schemes 4, 6, and 8, Supplementary Scheme 2, Table 1). For the 12-NO_2-LA regioisomer, the masses of the ions containing structural information were determined to be 157.1, 171.1, 195.1, and 213.1 (Figure 3A). Accurate mass determination revealed the presence of 8, 9, 11, and 11 carbons, respectively. The use of a ^{13}C standard (12-NO_2-[$^{13}C_{18}$] LA) confirmed the molecular composition for ion products *m/z* 165.1, 180.1, 206.1 and 224.1, respectively (Figure 3B). Loss of CO_2 was observed for these ion products upon MS^3 analysis. Thus, the analysis of 12-NO_2-LA corroborates the proposed neutral products depicted in the fragmentation schemes for 9-NO_2-LA and 10-NO_2-LA (Scheme 3).

Notably, the methylene-interrupted diene resulted in the formation and detection of two fragments containing either a carboxylic acid or an aldehyde, with the latter most likely derived from the carboxylic group by a loss of H_2O. However, the fragmentation of the 10-NO_2-OA only exhibited the formation of the aldehyde (*m/z* 169.1), suggesting that the additional exocyclic double bond on the carbon chain may favor the recyclization step (step 5, Scheme 5) or impair the formation of a reactive carbonyl peroxide upon fragmentation (step 3, Scheme 2).

13-NO_2-LA—The characteristic ions containing structural information of 13-NO_2-LA were identified with masses 171.1, 185.1, 227.1, and 209.1 (Figure 3C). Accurate mass determinations (<3 ppm) revealed the presence of 9, 10, 12, and 12 carbons, respectively. The molecular composition of these product ions was further confirmed by the analysis of a ^{13}C standard (13-NO_2-[$^{13}C_{18}$]LA), which showed the expected ions at *m/z* 180.1, 195.1, 239.2, and 221.2, respectively (Figure 3D). The fragmentation mechanism confirms the formation of five- and six-member heterocyclic rings and the formation of a carboxylic acid and an aldehyde upon fragmentation of the carbon chain. The 227.1 ion contains a

carboxylic acid moiety that undergoes rapid dehydration, with the subsequent formation of a ketenyl terminus (*m/z* 209.1). The fragmentation of 13-NO_2-LA revealed a similar fragmentation pattern as observed for 12-NO_2-LA, indicating that no conformational constraints affect the fragmentation pattern.

Fragmentation of $^{15}NO_2$-LA

To gain further insight and confirmation of the fragmentation mechanism of NO_2-LA, the four isomers of ^{15}N-containing NO_2-LA were fragmented and analyzed using high resolution mass spectrometry. All three major product ions having structural information for 9-NO_2-LA (*m/z* 168.1, 210.1 and 224.1) contain a nitrogen atom as evidenced by the shift in 1 Da observed upon 9-$^{15}NO_2$-LA fragmentation (yielding product ions with *m/z* 169.1, 211.1 and 225.1; Figure 4A). Similarly, the fragmentation of 10-$^{15}NO_2$-LA (Figure 4B) resulted in a shift of product ions of 14 with respect to 9-$^{15}NO_2$-LA (Figure 4A) and in a shift of 1 Da with respect of the fragments observed when 10-NO_2-LA was analyzed (Figure 2). These data confirm the fragments obtained and the presence of nitrogen in the product ions upon fragmentation in the 9- and 10-NO_2-LA isomers.

High resolution analysis of 12- and 13-NO_2-LA product ions did not provide evidence of the presence of nitrogen in the proposed structures (Figure 3). This was confirmed by fragmentation of 12- and 13-$^{15}NO_2$-LA (Figure 4C, D), which did not show a shift in the molecular mass of the chain breaking product ions with respect to 12- and 13-NO_2-LA. Thus, both 12-$^{15}NO_2$-LA and 12-NO_2-LA shared the same 157.1, 171.1, 195.1, and 213.1 *m/z* diagnostic ions and 13-$^{15}NO_2$-LA and 13-NO_2-LA shared the same 171.1, 185.1, 209.1, and 227.1 *m/z* diagnostic ions.

NO_2-SA and Reduced NO_2-LA

The presence of the nitroalkene was necessary to provide the electron density needed for net oxygen transfers to the carbon β to the nitro. Moreover, an additional double bond in the molecule allows an alternative pathway characterized by multiple cyclization pathways and the formation of stable five- or six-member rings. The fragmentation pathways of a *bis*-allylic interrupted nitroalkane-alkene were then tested. In this case, the electron density of the alkene was present but no double bond conjugation (nitroalkene) was available to accept the concerted flow of electrons necessary for intramolecular cyclization and oxygen transfer reactions. In this regard, CID fragmentation exhibited a major loss of 47 Da (neutral loss of HNO_2), a product ion of 46 *m/z* (NO_2^-) and almost no other product ions (Figure 5A). The fragmentation closely resembled the fragments obtained by SA-NO_2, in which a major loss of HNO_2 or formation of NO_2^- was observed (Figure 5B, C, Supplementary Scheme 3). Finally, it became clear that the unsaturation found in nitroalkenes is a necessary requirement for the observed fragmentation pathways. Moreover, the presence of an electronrich double bond in the γ- or δ-positions with respect to the NO_2 group did not modify the fragmentation products of nitroalkanes, thus demonstrating that the highly electron-withdrawn π electrons of the nitroalkene double bond (α, β- to the NO_2 group) actively participate in the oxygen transfer.

Fragmentation Yield Efficiencies for Specific Product Ions

The translation of this analysis into structural characterization for confirmation of biological NO_2-FA unknowns depends on the yields obtained during the fragmentation of the specific product ions. The slopes obtained for the *m/z* 324.2→46 standard curve for the four different NO_2-LA isomers were 1, representing a 100%. The data reported in Table 2 indicate efficiency yields (represented by the slopes of the standard curves with respect to the 324.2→46 transition) for specific product ions of up to 14%. Notably, the limit of detection (LOD), necessary to establish identity of the different isomers, was between 1.2 and 5 times

the calculated limit of quantification (LOQ) values for the highest product ion containing structural information for each isomer, further supporting both the theoretical and biological value of the method.

Conclusions

By evaluating the gas phase fragmentation products of nitroalkane and nitroalkene containing fatty acids, we propose several fragmentation pathways. These mechanisms provide the necessary elements for more insightful characterization of this class of labile and readily metabolized inflammatory signaling mediators. It has been previously observed that saturated aliphatic carbon chains containing nitro groups fragment via NO_2^- losses or HNO_2 neutral losses, rendering fragments with no structural information. Notably, the presence of a nitroalkene strongly favors both chain breaking fragmentation mechanisms as well as H_2O, HNO and NO_2^- losses [23]. The H_2O loss occurs at the NO_2 group, while the carboxylic acid retains the charge through the fragmentation process. In the case of monounsaturated nitroalkene fatty acids, the fragmentation mechanism involves an initial rearrangement followed by a retrocycloaddition and rupture to form fragments containing nitrile and aldehyde moieties. In particular, ions with *m/z* 168.1 and 169.1 indicate the presence of a double bond at position C9 and NO_2 groups at C9 and C10, respectively.

An unsaturation at positions δ- or γ- to the NO_2 group of the nitroalkene in polyunsaturated nitro fatty acids results in three major chain fragmentation pathways. These include nitrile and aldehyde products, as observed for monounsaturated nitroalkenes, and five- and six-member ring heterocycles. Several steps are involved in the formation of these species. In particular, fragmentation of 9-NO_2-LA results in specific ion fragments with *m/z* of 168.1, 210.1, and 224.1 with the latter showing a shift in 14 Da and having five- and six-member rings. The 10-NO_2-LA presented an overall shift of 14 Da compared with the fragments obtained from 9-NO_2-LA. The fragmentation of 12-NO_2-LA resulted in a different set of charged product ions characterized by *m/z* of 157.1, 171.1, 213.1, and 195.1. The difference in 14 Da between ions with *m/z* of 157.1 and 171.1 corresponds to the neutral formation of six- and five-member heterocycles (as observed for 9- and 10-NO_2-LA isomers). Finally, the fragmentation of 13-NO_2-LA shows an overall shift of 14 Da compared with 12-NO_2-LA with characteristic *m/z* of 171.1, 185.1, 227.1, and 209.1.

The efficiency of these product ions is between 0.2% and 14% of the maximal fragmentation obtained when following the formation of a 46 product ion (NO_2^-). The LOD of these fragments is between 1.2 and 5 times the LOQ, underlining the potential and applicability of this technique to the analysis of isomers in biological samples.

Supplementary Material

Refer to Web version on PubMed Central for supplementary material.

Acknowledgments

The authors thank Paul R. S. Baker, Ph.D. for useful discussions. This study was supported by an USPHS grant R01DA027806 and a Department of Education grant P116Z090309 (to E.K.A.), a Junior Faculty Award 7-08-JF-52 American Diabetes Association (to F.J.S.), and R01 HL58115 and R01 HL64937 (to B.A.F., F.J.S.).

Abbreviations

CID	Collision induced dissociation
NO_2-FA	Nitro-fatty acids

NO_2-SA	nitrated stearic acid
NO_2-OA	nitrated oleic acid
NO_2-LA	nitrated linoleic acid
9-NO_2-OA	9-nitro-octadeca-9-enoic acid
10-NO_2-OA	10-nitro-octadeca-9-enoic acid
9-NO_2-LA	9-nitro-octadeca-9,12-dienoic acid
10-NO_2-LA	10-nitro-octadeca-9,12-dienoic acid
12-NO_2-LA	12-nitro-octadeca-9,12-dienoic acid
13-NO_2-LA	13-nitro-octadeca-9,12-dienoic acid
9-NO_2-SA	9-nitro-octadecanoic acid
10-NO_2-SA	10-nitro-octadecanoic acid
ZPE	Zero point vibrational energies
LOD	limit of detection
LOQ	limit of quantification

References

1. O'Donnell VB, Eiserich JP, Chumley PH, Jablonsky MJ, Krishna NR, Kirk M, Barnes S, Darley-Usmar VM, Freeman BA. Nitration of Unsaturated Fatty Acids by Nitric Oxide-Derived Reactive Nitrogen Species Peroxynitrite, Nitrous Acid, Nitrogen Dioxide, and Nitronium ion. Chem. Res. Toxicol. 1999; 12:83–92. [PubMed: 9894022]
2. Rubbo H, Parthasarathy S, Barnes S, Kirk M, Kalyanaraman B, Freeman BA. Nitric Oxide Inhibition of Lipoxygenase-Dependent Liposome and Low-Density Lipoprotein Oxidation: Termination of Radical Chain Propagation Reactions and Formation of Nitrogen-Containing Oxidized Lipid Derivatives. Arch. Biochem. Biophys. 1995; 324:15–25. [PubMed: 7503550]
3. Baker PR, Lin Y, Schopfer FJ, Woodcock SR, Groeger AL, Batthyany C, Sweeney S, Long MH, Iles KE, Baker LM, Branchaud BP, Chen YE, Freeman BA. Fatty Acid Transduction of Nitric Oxide Signaling: Multiple Nitrated Unsaturated Fatty Acid Derivatives Exist in Human Blood and Urine and Serve as Endogenous Peroxisome Proliferator-Activated Receptor Ligands. J Biol. Chem. 2005; 280:42464–42475. [PubMed: 16227625]
4. Baker PR, Schopfer FJ, Sweeney S, Freeman BA. Red Cell Membrane and Plasma Linoleic Acid Nitration Products: Synthesis, Clinical Identification, and Quantitation. Proc. Natl. Acad. Sci. USA. 2004; 101:11577–11582. [PubMed: 15273286]
5. Lima ES, Di Mascio P, Abdalla DS. Cholesteryl Nitrolinoleate, a Nitrated Lipid Present in Human Blood Plasma and Lipoproteins. J. Lipid Res. 2003; 44:1660–1666. [PubMed: 12837858]
6. Rudolph V, Rudolph TK, Schopfer FJ, Bonacci G, Woodcock SR, Cole MP, Baker PR, Ramani R, Freeman BA. Endogenous Generation and Protective Effects of Nitro-Fatty Acids in a Murine Model of Focal Cardiac Ischemia and Reperfusion. Cardiovasc. Res. 2010; 85:155–166. [PubMed: 19666678]
7. Tsikas D, Zoerner A, Mitschke A, Homsi Y, Gutzki FM, Jordan J. Specific GC-MS/MS Stable-Isotope Dilution Methodology for Free 9- and 10-Nitro-Oleic Acid in Human Plasma Challenges Previous LC-MS/MS Reports. J. Chromatogr. B Analyt. Technol. Biomed. Life Sci. 2009; 877:2895–2908.
8. Tsikas D, Zoerner AA, Mitschke A, Gutzki FM. Nitro-Fatty Acids Occur in Human Plasma in the Picomolar Range: A Targeted Nitro-Lipidomics GC-MS/MS Study. Lipids. 2009; 44:855–865. [PubMed: 19701657]

9. Schopfer FJ, Lin Y, Baker PR, Cui T, Garcia-Barrio M, Zhang J, Chen K, Chen YE, Freeman BA. Nitrolinoleic Acid: An Endogenous Peroxisome Proliferator-Activated Receptor γ ligand. Proc. Natl. Acad. Sci. USA. 2005; 102:2340–2345. [PubMed: 15701701]
10. Kansanen E, Jyrkkanen HK, Volger OL, Leinonen H, Kivela AM, Hakkinen SK, Woodcock SR, Schopfer FJ, Horrevoets AJ, Yla-Herttuala S, Freeman BA, Levonen AL. Nrf2-Dependent and -Independent Responses to Nitro-Fatty Acids in Human Endothelial Cells: Identification of Heat Shock Response as the Major Pathway Activated by Nitro-Oleic Acid. J. Biol. Chem. 2009; 284:33233–33241. [PubMed: 19808663]
11. Cui T, Schopfer FJ, Zhang J, Chen K, Ichikawa T, Baker PR, Batthyany C, Chacko BK, Feng X, Patel RP, Agarwal A, Freeman BA, Chen YE. Nitrated Fatty Acids: Endogenous Anti-Inflammatory Signaling mediators. J. Biol. Chem. 2006; 281:35686–35698. [PubMed: 16887803]
12. Liu W, Morrow JD, Yin H. Quantification of F2-Isoprostanes as a Reliable Index of Oxidative Stress In Vivo Using Gas Chromatography-Mass Spectrometry (GC-MS) Method. Free Radic. Biol. Med. 2009; 47:1101–1107. [PubMed: 19647073]
13. Nadtochiy SM, Baker PR, Freeman BA, Brookes PS. Mitochondrial Nitroalkene Formation and Mild Uncoupling in Ischaemic Preconditioning: Implications for Cardioprotection. Cardiovasc. Res. 2009; 82:333–340. [PubMed: 19050010]
14. Rudolph V, Schopfer FJ, Khoo NK, Rudolph TK, Cole MP, Woodcock SR, Bonacci G, Groeger AL, Golin-Bisello F, Chen CS, Baker PR, Freeman BA. Nitro-Fatty Acid Metabolome: Saturation, Desaturation, β-Oxidation, and Protein Adduction. J. Biol. Chem. 2009; 284:1461–1473. [PubMed: 19015269]
15. Baker LM, Baker PR, Golin-Bisello F, Schopfer FJ, Fink M, Woodcock SR, Branchaud BP, Radi R, Freeman BA. Nitro-Fatty Acid Reaction with Glutathione and Cysteine. Kinetic Analysis of Thiol Alkylation by a Michael Addition Reaction. J. Biol. Chem. 2007; 282:31085–31093. [PubMed: 17720974]
16. Ferreira AM, Ferrari MI, Trostchansky A, Batthyany C, Souza JM, Alvarez MN, Lopez GV, Baker PR, Schopfer FJ, O'Donnell V, Freeman BA, Rubbo H. Macrophage Activation Induces Formation of the Anti-Inflammatory Lipid Cholesteryl-Nitrolinoleate. Biochem. J. 2009; 417:223–234. [PubMed: 18671672]
17. Ferreira AM, Trostchansky A, Ferrari M, Souza JM, Rubbo H. Nitroalkenes: Synthesis, Characterization, and Effects on Macrophage Activation. Methods Enzymol. 2008; 441:33–51. [PubMed: 18554528]
18. Kelley EE, Batthyany CI, Hundley NJ, Woodcock SR, Bonacci G, Del Rio JM, Schopfer FJ, Lancaster JR Jr. Freeman BA, Tarpey MM. Nitro-Oleic Acid, a Novel and Irreversible Inhibitor of Xanthine Oxidoreductase. J. Biol. Chem. 2008; 283:36176–36184. [PubMed: 18974051]
19. Batthyany C, Schopfer FJ, Baker PR, Duran R, Baker LM, Huang Y, Cervenansky C, Branchaud BP, Freeman BA. Reversible Post-Translational Modification of Proteins by Nitrated Fatty Acids In Vivo. J. Biol. Chem. 2006; 281:20450–20463. [PubMed: 16682416]
20. Gorczynski MJ, Smitherman PK, Akiyama TE, Wood HB, Berger JP, King SB, Morrow CS. Activation of Peroxisome Proliferator-Activated Receptor γ (PPARγ) by Nitroalkene Fatty Acids: Importance of Nitration Position and Degree of Unsaturation. J. Med. Chem. 2009; 52:4631–4639. [PubMed: 19719236]
21. Li Y, Zhang J, Schopfer FJ, Martynowski D, Garcia-Barrio MT, Kovach A, Suino-Powell K, Baker PR, Freeman BA, Chen YE, Xu HE. Molecular Recognition of Nitrated Fatty Acids by PPARγ. Nat. Struct. Mol. Biol. 2008; 15:865–867. [PubMed: 18604218]
22. Balazy M, Iesaki T, Park JL, Jiang H, Kaminski PM, Wolin MS. Vicinal Nitrohydroxyeicosatrienoic Acids: Vasodilator Lipids Formed by Reaction of Nitrogen Dioxide with Arachidonic acid. J. Pharmacol. Exp. Ther. 2001; 299:611–619. [PubMed: 11602673]
23. Jain K, Siddam A, Marathi A, Roy U, Falck JR, Balazy M. The Mechanism of Oleic Acid Nitration by *NO(2). Free Radic. Biol. Med. 2008; 45:269–283. [PubMed: 18457679]
24. Trostchansky A, Souza JM, Ferreira A, Ferrari M, Blanco F, Trujillo M, Castro D, Cerecetto H, Baker PR, O'Donnell VB, Rubbo H. Synthesis, Isomer Characterization, and Anti-Inflammatory Properties of Nitroarachidonate. Biochemistry. 2007; 46:4645–4653. [PubMed: 17373826]

25. Attygalle AB, Ruzicka J, Varughese D, Bialecki JB, Jafri S. Low-energy collision-induced fragmentation of negative ions derived from ortho-, meta-, and para-hydroxyphenyl carbaldehydes, ketones, and related compounds. J. Mass Spectrom. 2007; 42:1207–1217. [PubMed: 17694503]
26. Schymanski EL, Meringer M, Brack W. Matching Structures to Mass Spectra Using Fragmentation Patterns: Are the Results as Good as They Look? Anal. Chem. 2009; 81:3608–3617. [PubMed: 19323534]
27. Woodcock SR, Marwitz AJV, Bruno P, Branchaud BP. Synthesis of Nitrolipids. All Four Possible Diastereomers of Nitrooleic Acids: (E)- and (Z)-, 9-, and 10-Nitro-Octadec-9-Enoic Acids. Org. Lett. 2006; 8:3931–3934. [PubMed: 16928041]
28. MOE. Chemical Computing Group, Inc.; Montreal:
29. Stewart JP. Optimization of Parameters for Semiempirical Methods I. Method. J. Comp. Chem. 1989; 10:209–220.
30. Frisch, MJTGW.; Schlegel, HB.; Scuseria, GE.; Robb, MA.; Cheeseman, JR.; Scalmani, G.; Barone, V.; Mennucci, B.; Petersson, GA.; Nakatsuji, H.; Caricato, M.; Li, X.; Hratchian, HP.; Izmaylov, AF.; Bloino, J.; Zheng, G.; Sonnenberg, JL.; Hada, M.; Ehara, M.; Toyota, K.; Fukuda, R.; Hasegawa, J.; Ishida, M.; Nakajima, T.; Honda, Y.; Kitao, O.; Nakai, H.; Vreven, T.; Montgomery, JA., Jr.; Peralta, JE.; Ogliaro, F.; Bearpark, M.; Heyd, JJ.; Brothers, E.; Kudin, KN.; Staroverov, VN.; Kobayashi, R.; Normand, J.; Raghavachari, K.; Rendell, A.; Burant, JC.; Iyengar, SS.; Tomasi, J.; Cossi, M.; Rega, N.; Millam, NJ.; Klene, M.; Knox, JE.; Cross, JB.; Bakken, V.; Adamo, C.; Jaramillo, J.; Gomperts, R.; Stratmann, RE.; Yazyev, O.; Austin, AJ.; Cammi, R.; Pomelli, C.; Ochterski, JW.; Martin, RL.; Morokuma, K.; Zakrzewski, VG.; Voth, GA.; Salvador, P.; Dannenberg, JJ.; Dapprich, S.; Daniels, AD.; Farkas, Ö.; Foresman, JB.; Ortiz, JV.; Cioslowski, J.; Fox, DJ. Gaussian 09, Revision. Gaussian, Inc.; 2009.
31. Schopfer FJ, Batthyany C, Baker PR, Bonacci G, Cole MP, Rudolph V, Groeger AL, Rudolph TK, Nadtochiy S, Brookes PS, Freeman BA. Detection and Quantification of Protein Adduction by Electrophilic Fatty Acids: Mitochondrial Generation of Fatty Acid Nitroalkene Derivatives. Free Radic. Biol. Med. 2009; 46:1250–1259. [PubMed: 19353781]
32. Alexander RL, Wright MW, Gorczynski MJ, Smitherman PK, Akiyama TE, Wood HB, Berger JP, King SB, Morrow CS. Differential Potencies of Naturally Occurring Regioisomers of Nitrolinoleic Acid in PPARγ activation. Biochemistry. 2009; 48:492–498. [PubMed: 19105608]

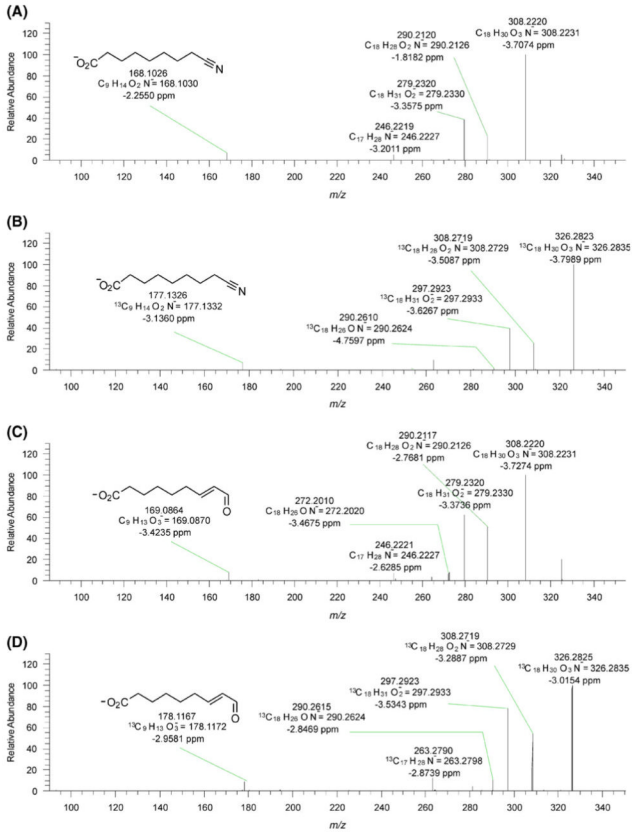

Figure 1.

Product ion spectra of $[M - H]^-$ ions of *m/z* 326.3 and 344.3 corresponding to NO_2-OA and NO_2-[$^{13}C_{18}$]OA, respectively. (**A**) 9-NO_2-OA, (**B**) 9-NO_2-[$^{13}C_{18}$]OA, (**C**) 10-NO_2-OA, (**D**) 10-NO_2-[$^{13}C_{18}$]OA recorded at a collision energy setting of 35 eV using a hybrid FT mass spectrometer

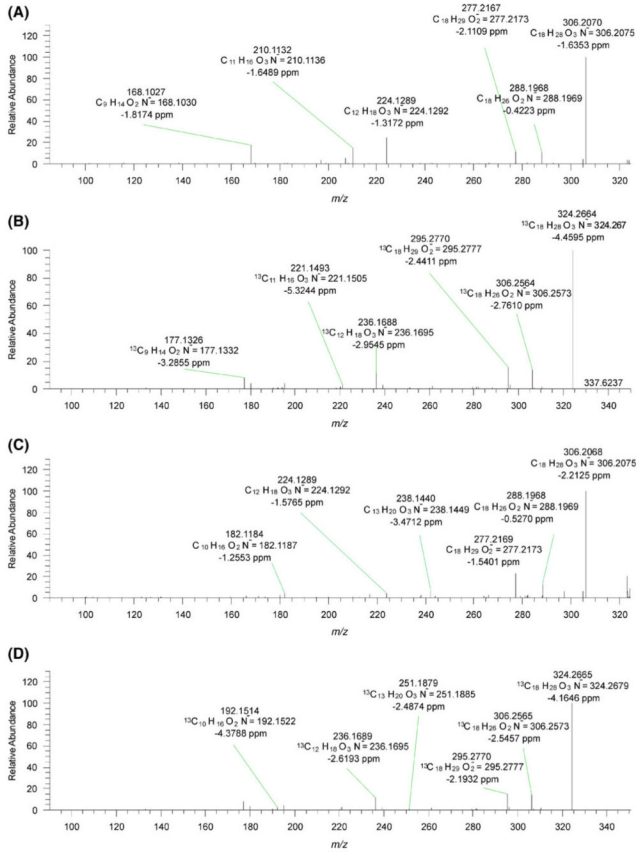

Figure 2.

Product ion spectra of $[M - H]^-$ ions of *m/z* 324.2 and 342.3 corresponding to NO_2-LA and NO_2-[$^{13}C_{18}$]LA respectively. (**A**) 9-NO_2-LA, (**B**) 9-NO_2-[$^{13}C_{18}$]LA, (**C**) 10-NO_2-LA, (**D**) 10-NO_2-[$^{13}C_{18}$]LA recorded at a collision energy setting of 35 eV using a hybrid FT mass spectrometer

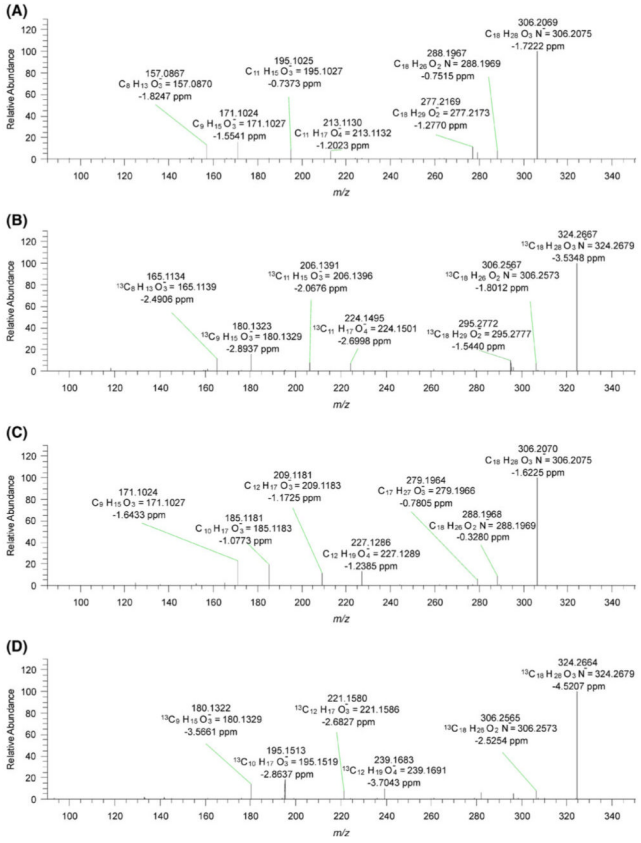

Figure 3.

Product ion spectra of $[M - H]^-$ ions of *m/z* 324.2 and 342.3 corresponding to NO_2-LA and NO_2-[$^{13}C_{18}$]LA, respectively. (**A**) 12-NO_2-LA, (**B**) 12-NO_2-[$^{13}C_{18}$]LA, (**C**) 13-NO_2-LA, (**D**) 13-NO_2-[$^{13}C_{18}$]LA recorded at a collision energy setting of 35 eV using a hybrid FT mass spectrometer

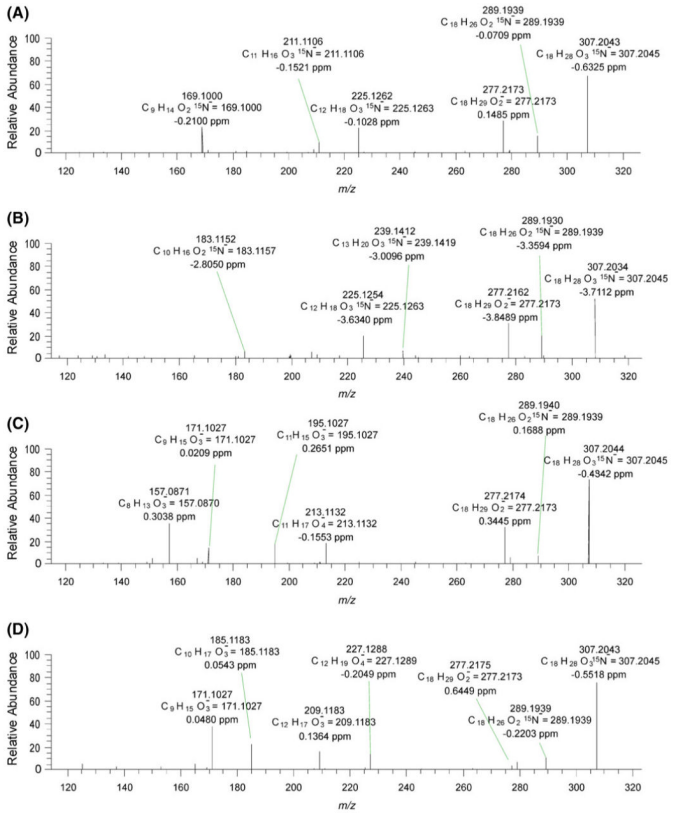

Figure 4.

Product ion spectra of $[M - H]^-$ ions of *m/z* 325.3 corresponding to $^{15}NO_2$-LA. (**A**) 9-$^{15}NO_2$-LA, (**B**) 10-$^{15}NO_2$-LA, (**C**) 12-$^{15}NO_2$-LA, (**D**) 13-$^{15}NO_2$-LA recorded at a collision energy setting of 35 eV using a hybrid FT mass spectrometer

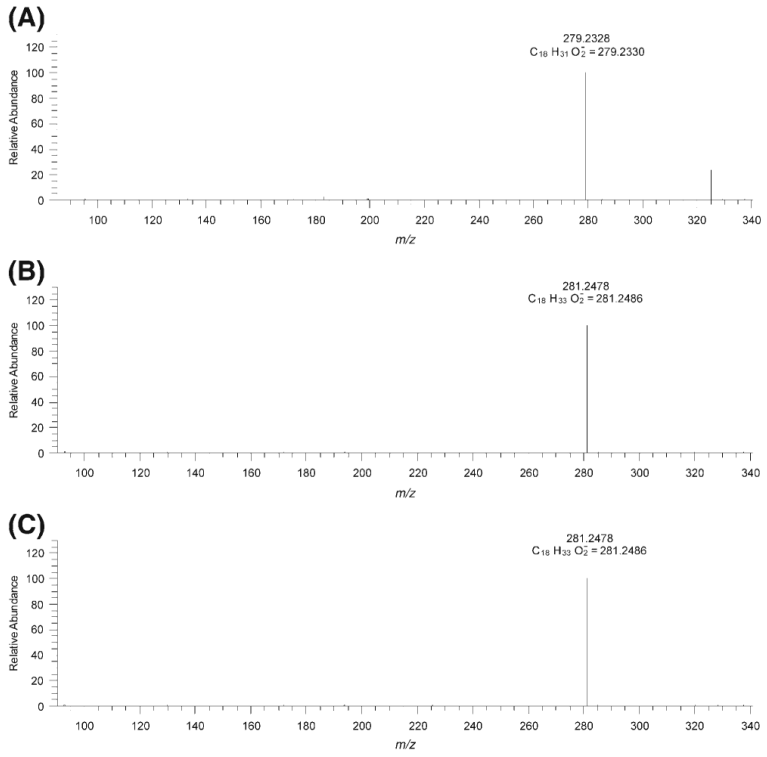

Figure 5.

Product ion spectra of $[M - H]^-$ ions of *m/z* 326.3 and 328.3 corresponding to reduced NO_2-LA (nitroalkane alkene containing NO_2-OA) and reduced NO_2-OA (nitrostearic acid, SA-NO_2) respectively. (**A**) reduced NO_2-LA (*m/z* 326.3), (**B**) 10-NO_2-SA (*m/z* 328.3), (**C**) 9-NO_2-SA (*m/z* 328.3) recorded at a collision energy setting of 35 eV using a hybrid FT mass spectrometer

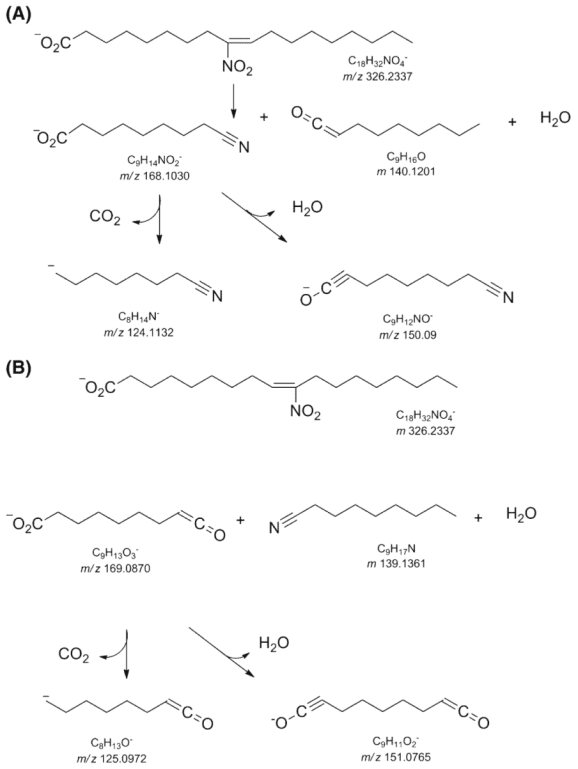

Scheme 1.

Fragmentation products of 9-NO_2-OA and 10-NO_2-OA. (**A**) Fragmentation of 9-NO_2-OA results in a characteristic ion with *m/z* 168.1, which can be further fragmented to elicit neutral losses of H_20 and CO_2. (**B**) Fragmentation of 10-NO_2-OA results in a product ion *m/z* 169.1, which displays losses of H_2O and CO_2 in MS^3 fragmentations

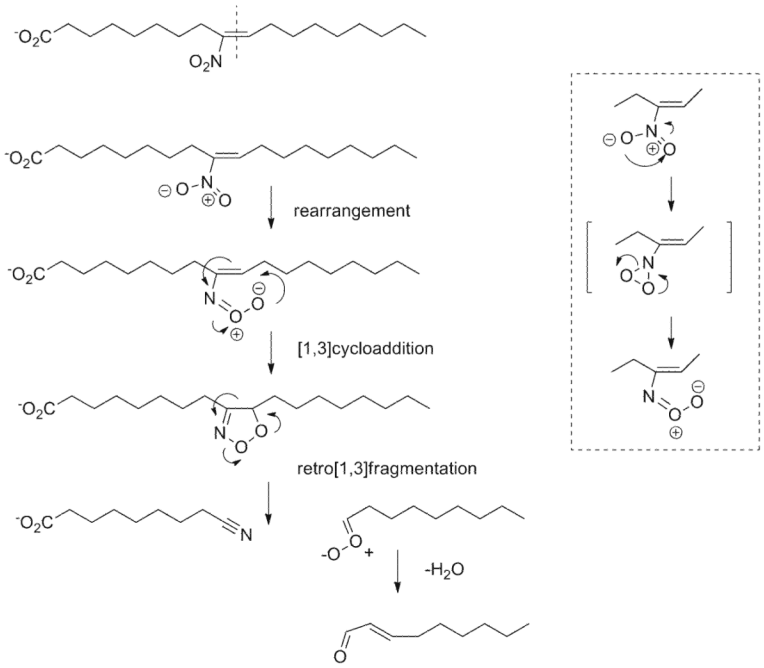

Scheme 2.

Proposed fragmentation mechanism of 9-NO_2-OA. The fragmentation proceeds through a series of steps that include rearrangement, 1,3-cycloaddition and a final retro-1,3-fragmentation to a nitrile and corresponding unsaturated aldehyde. Sidebar: potential rearrangement of nitro group to hypothesized peroxynitroso intermediate

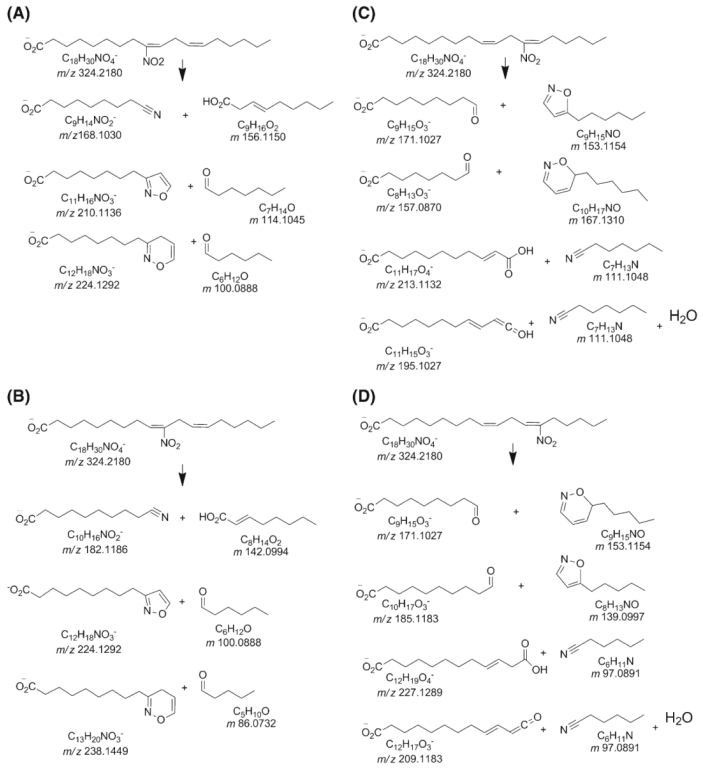

Scheme 3.

Proposed product ions, containing structural information, and their respective neutral fragments of the gas phase fragmentation of 4 positional nitroalkene isomers. (**A**) 9-NO_2-LA, (**B**) 10-NO_2-LA, (**C**) 12-NO_2-LA, (**D**) 13-NO_2-LA

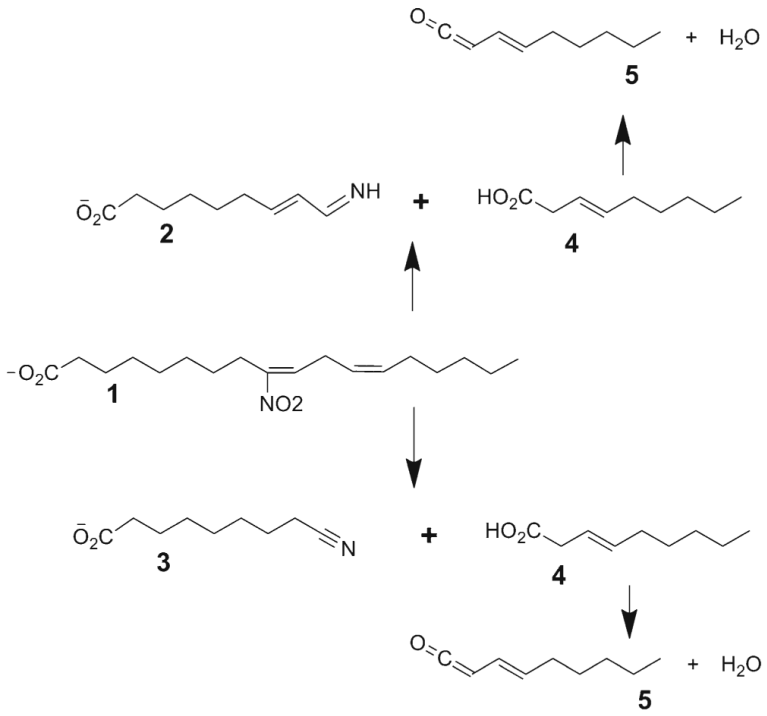

Scheme 4.

Principal candidates of product ion and neutral losses obtained after fragmentation of 9-NO_2-LA to form a nitrile containing ion. Ions 2 and 3 were selected for accurate free energy determinations because they displayed the lowest energies during semiempirical product ion calculations. Free energies are shown in Table 1. Ion 3 is the proposed ion products obtained during fragmentation

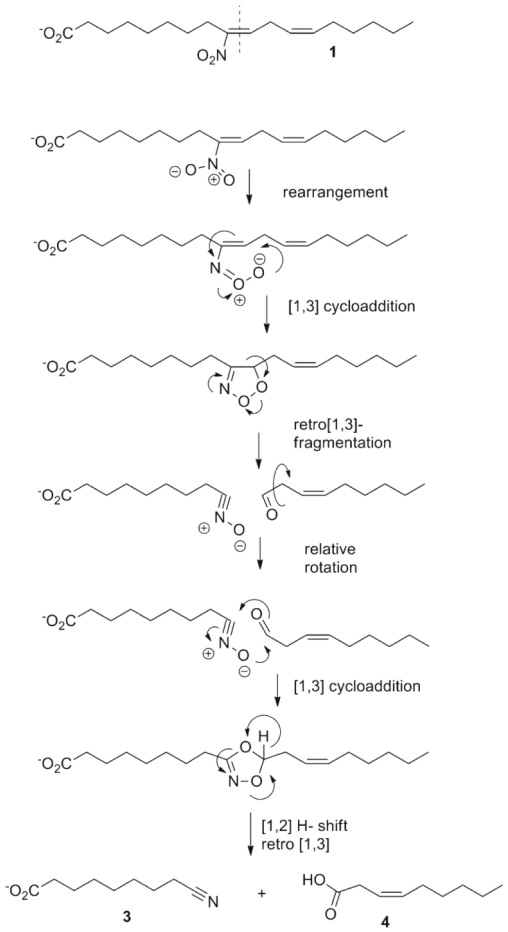

Scheme 5.

Proposed fragmentation pathway of 9-NO_2-LA. Product ion 3 and neutral loss 4 were selected because they display the lowest free energy

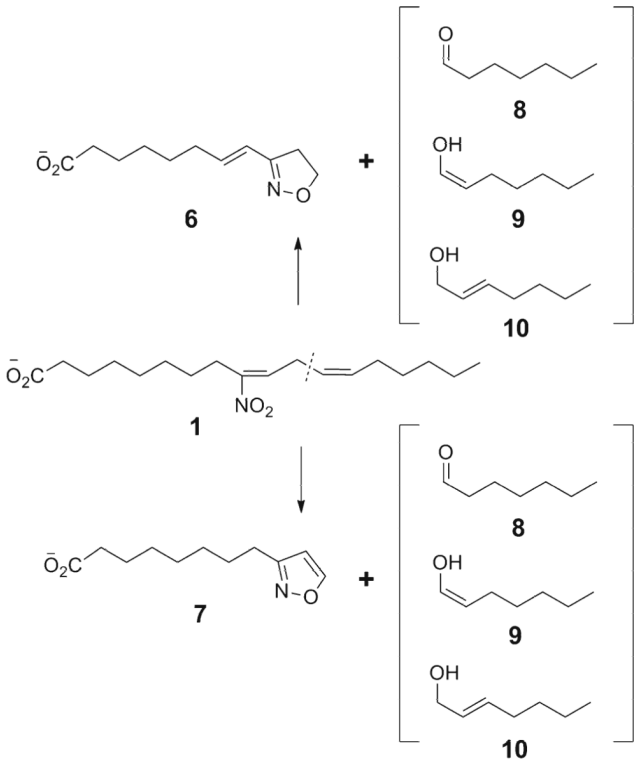

Scheme 6.

Main candidates of product ion and neutral losses obtained after fragmentation of 9-NO_2-LA to form a five-member heterocycle. Ions 6 and 7 were selected for accurate free energy determinations because they displayed the lowest energies during semiempirical product ion calculations. Free energies are shown in Table 1. Ion 7 is the proposed ion products obtained during fragmentation in addition to the neutral fragment 8

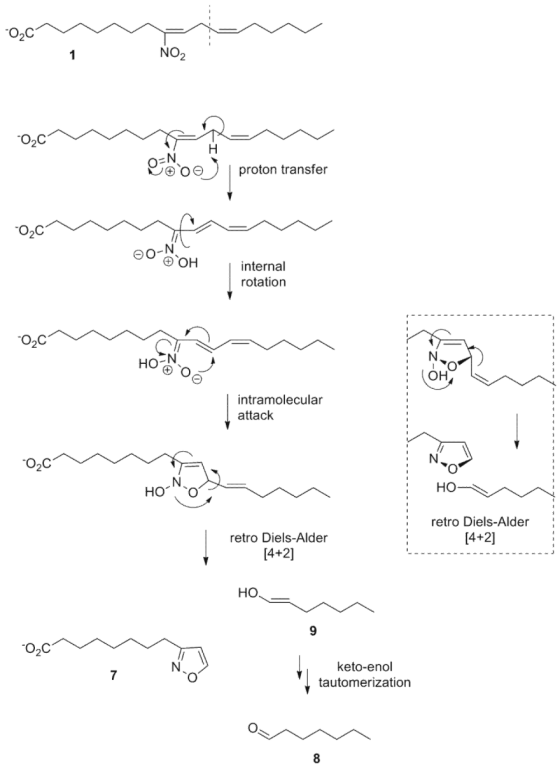

Scheme 7.

Proposed fragmentation pathway of 9-NO_2-LA to form the pentacycle containing product ion. Product ion 7 and neutral loss 8 displayed the lowest free energy compared with other products

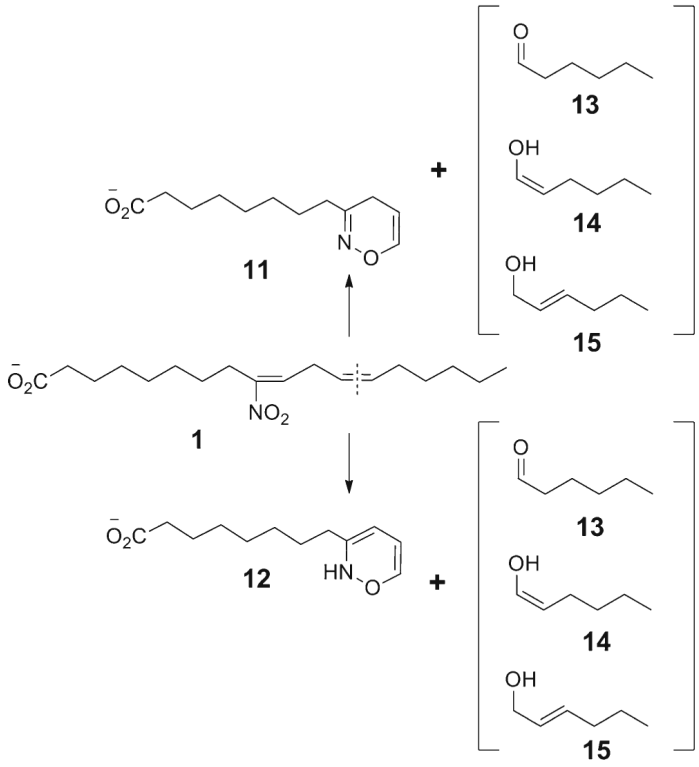

Scheme 8.

Main candidates for product ion and neutral losses obtained after fragmentation of 9-NO_2-LA to form a hexacycle. Ions 11 and 12 were selected from accurate free energy determinations because they displayed the lowest energies during semiempirical product ion calculations. Free energies are shown in Table 1. Ion 11 is the proposed ion products obtained during fragmentation in addition to the neutral fragment 13. Neutral fragment 13 is a methylene group shorter than neutral ion 8 formed during fragmentation rendering the five-member heterocycle

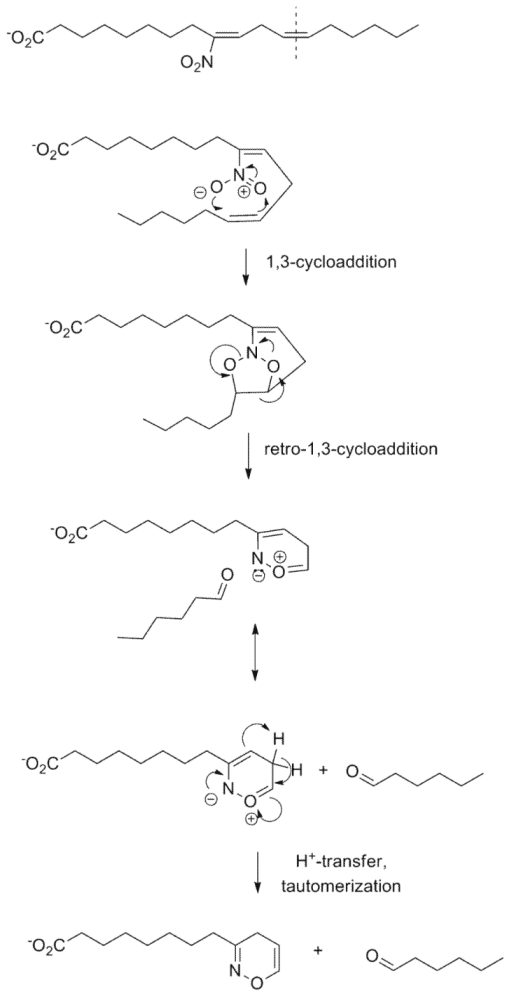

Scheme 9.

Proposed fragmentation pathway of 9-NO_2-LA to form the hexacyclic product ion. Product ion 11 and neutral loss 13 displayed the lowest free energy compared with other possible products

Table 1

Total and relative energies for the 15 tested structures. Energies were calculated using the B3LYP method and 6-311G basis set. Zero point energy corrections were applied. The displayed ΔE represents the energy difference compared to the structure with lowest energy value (assigned as 0) of each structural group. Groups are represented by Structures 2–3, 4–5, 6–7, 8–10, 11–12, and 13–15

Structure	Electronic+thermal energy at 298 K (kcal/mol)	ΔE(kcal/mol)
2	−349121.24	16.1
3	−349137.30	0
4	−315491.38	0
5	−267529.07	47962.3
6	−444844.96	12.3
7	−444857.24	0
8	−195089.64	0
9	−195080.37	9.3
10	−195077.75	11.9
11	−469491.61	0
12	−469481.97	9.6
13	−219739.58	0
14	−219730.34	9.2
15	−219727.71	11.9

Table 2

Efficiency of MRM specific transitions for LA-NO_2 and OA-NO_2. The efficiency is expressed relative to the maximum signal obtained, which corresponds to the fragmentation following the formation of the NO_2^- product ion (324.2→46 and 326.2→46 for LA-NO_2 and OA-NO_2, respectively)

MRM transition	Product ion efficiency (%)
9-NO2-LA	
324.2 → 46	100
324.2 → 168.1	7.9
324.2 → 210.1	1.5
324.2 → 224.1	3.3
10-NO2-LA	
324.2 → 46	100
324.2 → 182.1	1.3
324.2 → 224.1	3.3
324.2 → 238.1	0.2
12-NO2-LA	
324.2 → 46	100
324.2 → 157.1	7.3
324.2 → 171.1	14.2
324.2 → 195.1	1.4
324.2 → 213.1	0.8
13-NO2-LA	
324.2 → 46	100
324.2 → 171.1	14.1
324.2 → 185.1	8.2
324.2 → 209.1	4.8
324.2 → 227.1	2.8
9-NO2-OA	
326.2 → 46	100
326.2 → 168.1	4.6
10-NO2-OA	
324.2 → 46	100
326.2 → 169.1	2.0